Measurement and Assessment of Fatigue Life of Spot-Weld Joints

Ahmet H. Ertas
Department of Mechanical Engineering,
Bogazici University,
Bebek,
Istanbul 34342, Turkey

Oktem Vardar
Isik University,
Sile,
Istanbul 34398, Turkey

Fazil O. Sonmez
Department of Mechanical Engineering,
Bogazici University,
Bebek,
Istanbul 34342, Turkey
e-mail: sonmezfa@boun.edu.tr

Zafer Solim
Mercedes-Benz Turk A.S.,
Bahcesehir,
Istanbul 34500, Turkey

Spot-weld joints are commonly used to fasten together metal sheets. Because fatigue fracture is the most critical failure mode for these joints under fluctuating loads, understanding their fatigue failure behavior and assessment of their fatigue lives are crucial from the viewpoint of failure prevention in design. In this study, a series of experiments was conducted to study the fatigue failure of spot-welded modified tensile-shear specimens made of a low carbon steel. Two different types of resistance spot welding were investigated (manual and automated). Tests were repeated under different load ranges, and the corresponding fatigue lives were determined. The specimens were also examined under an optical microscope. In the numerical part of this study, a finite element analysis was carried out using commercial software, ANSYS, to determine the stress and strain states within the specimens. The material nonlinearity, local plastic deformations around the welds during loading, and the residual stresses and strains developed after unloading as a result of plastic deformations were taken into account. Based on the predicted stress and strain states, fatigue analyses were performed using several models for life assessment. Then, the measured and predicted fatigue lives were compared, and the suitability of the models was discussed. Among the strain-based models, Coffin–Manson and Morrow's means stress models yielded the best predictions. [DOI: 10.1115/1.3030941]

Keywords: fatigue fracture, modified tensile-shear (MTS) specimen, spot weld, FEM, low carbon steel

1 Introduction

Despite the availability of other joining methods such as laser beam welding and adhesive bonding, resistance spot welding remains the primary method for joining panels and bodies especially in automobile, railroad, and airplane structures. The economical advantages of spot welding were understood many years ago by the aerospace industry [1]. About 90% of the welds used in an automotive body assembly are resistance spot welds [2]. A typical vehicle contains more than 3000 spot welds [3–8]. This number may reach 5000 and sometimes 8000 in bus and coach bodies. The advantages of using spot welds are that the joining process is faster, no filler material is required, and dimensional accuracy is better preserved during welding with local heating [3–6,8–10].

In service, mechanical components usually experience cyclic loading. This makes fatigue failure prevention the foremost design requirement. Considering that spot welds provide localized connection, thus creating inherent circumferential notches, they lead to stress concentrations and consequently make the structure more likely to fail due to fatigue. For instance, approximately 80% of all cases of fatigue failure in automotive components occur around a spot weld; 15% of them at a low-quality-cut edge, and only in 5% fatigue cracks initiate in sheet metal [11]. Accordingly, one may assume that under normal service conditions, fatigue strength of spot-weld joints dominates the overall structural durability. Hence, a better understanding of spot-weld fatigue behavior and use of reliable fatigue assessment models should be considered as the requirements for reliable designs. For this reason, many researchers [2–4,10–25] have focused on this subject.

A deeper understanding of the fatigue behavior can be attained through further experiments and observations. Basic fatigue characterization tests were commonly conducted using tensile-shear (TS) specimens [2,3,5,8,10,13,14,18,22,26], which contain two or three plates joined by one or two spot welds loaded in shear. On the other hand, modified tensile-shear (MTS) specimens, which contain plates bent at their longitudinal edges, were rarely studied. MTS specimens have higher flexural stiffness and thus have higher resistance to bending and buckling. For this reason, this type of geometry is more commonly used in industrial applications. Although TS and MTS specimens are loaded uniaxially in fatigue tests, plates are subject to bending moment due to eccentricity. Higher flexural stiffness of MTS will therefore have an impact on fatigue life. However, there are a few experimental data [18] available on fatigue behavior of MTS. In this study, fatigue failure tests were conducted on MTS specimens to understand their fatigue failure behavior as in Ref. [18]; but a different material, geometry, and R-ratio were used.

There are basically two types of spot welds, namely, automated (or standard) and manual. An automated-type spot weld is produced by holding the plates from both faces with two pincers while applying force and transmitting current. A manual spot weld is materialized by touching the electrode on one surface of the specimen without applying force. This type of spot weld may be preferred in some industrial applications if the sheets cannot be gripped at both sides. The studies on fatigue strength of spot-welded joints focused on automated-type spot welds. In this study, automated-type as well as manual-type spot welds were investigated experimentally, and the range of difference in their life spans was compared.

Even if plates joined by spot welds are subject to uniaxial in-plane loads, multiaxial stresses develop around the spot welds. Due to the high stress concentration, plastic deformation is likely to occur around the welds. These stresses control the useful life of the joint and thus the specimen. For a reliable fatigue life assessment, one is required to determine, first of all, the stress field around the spot weld accurately. In this study, a nonlinear finite element analysis (FEA) was carried out using nonlinear material properties and contact elements on the inner surfaces of the plates to find the stress and strain states. Plastic deformation and residual stresses developed after unloading were determined and accounted for in calculating the range of stress and strain fluctuations.

Contributed by the Materials Division of ASME for publication in the JOURNAL OF ENGINEERING MATERIALS AND TECHNOLOGY. Manuscript received February 14, 2008; final manuscript received October 11, 2008; published online December 22, 2008. Assoc. Editor: Pedro Peralta.

Copyright © 2009 by ASME

Downloaded 26 Dec 2008 to 193.140.210.85. Redistribution subject to ASME license or copyright; see http://www.asme.org/terms/Terms_Use.cfm

Another requirement for accurate fatigue life predictions is to use a reliable fatigue failure model. Different approaches are available for fatigue life assessment such as the nominal stress approach, the structural or hot-spot stress approach [17], the notch stress approach considering stress concentration effects and notch intensity [15,18,21,27,28], the notch strain approach [18,21,27,29–31], volumetric fatigue approach [18,25], and finally the crack propagation or fracture mechanics approach [10,18,21,28,32–34]. In this study, instead of using a fatigue model specifically developed for spot welds as in the previous studies, applicability of general fatigue models was investigated. It is more desirable for a designer to use a single model generally applicable to all types of connections rather than using a separate model for each one of them. For this purpose a number of general purpose fatigue models were utilized to decide on which one of them would provide the best predictions for a spot-weld joint.

2 Models for Fatigue Life Prediction

Various fatigue life prediction criteria have been suggested in literature. They are classified as strain-based and stress-based approaches in general.

2.1 Stress-Based Approaches. These are based on the assumption that the range of values for stress controls the fatigue behavior of a component. They involve empirical relations between uniaxial fully reversed stress and fatigue life (*S-N* curves). However, mechanical components are usually subject to stresses oscillating about an average stress level. For these cases, a number of models were proposed.

$$\frac{S_a}{S_f} + \frac{S_m}{S_{\text{ut}}} = 1 \quad \text{(modified Goodman, England, 1899)} \tag{1}$$

$$\frac{S_a}{S_f} + \left(\frac{S_m}{S_{\text{ut}}}\right)^2 = 1 \quad \text{(Gerber, Germany, 1874)} \tag{2}$$

$$\frac{S_a}{S_f} + \frac{S_m}{S_y} = 1 \quad \text{(Soderberg, USA, 1930)} \tag{3}$$

$$\frac{S_a}{S_f} + \frac{S_m}{\sigma_f} = 1 \quad \text{(Morrow, USA, 1960s)} \tag{4}$$

where S_a is the alternating stress, S_m is the mean stress, S_f is the fully reversed fatigue strength of the material, S_{ut} is the ultimate tensile strength, S_y is the yield strength, and σ_f is the true fracture strength, i.e., the true stress at final fracture. If a structure is subject to multiaxial stress state, equivalent uniaxial alternating and mean stresses can be used in fatigue calculations for proportional loading cases. The loading case considered in this study was assumed to be proportional. Otherwise, more sophisticated models like critical plane approaches should be adopted.

2.2 Strain-Based Approaches. According to these models, the range of values for strain controls the fatigue life. They also take into account the effect of plastic strain. They are, therefore, especially suitable for cases where plastic effects dominate the fatigue behavior. Although most engineering structures and components are designed such that nominal stresses remain elastic, stress concentrations often cause plastic strains to develop in the vicinity of notches, e.g., spot welds in our case. Fatigue cracks usually nucleate due to plastic straining at the notches. The total strain amplitude can be resolved into elastic and plastic strain components, each of which has been shown to be correlated with fatigue life via power-law relationships for most metals [35]. The local notch strain approach (or Coffin–Manson relationship) relates alternating true elastic and plastic strains, $\Delta\varepsilon_e$ and $\Delta\varepsilon_p$, to fatigue life, that is, the number of cycles to failure (N_f), as follows [35,36]:

$$\frac{\Delta\varepsilon}{2} = \frac{\Delta\varepsilon_e}{2} + \frac{\Delta\varepsilon_p}{2} = \frac{\sigma_f'}{E}(2N_f)^b + \varepsilon_f'(2N_f)^c \tag{5}$$

where σ_f' is the fatigue strength coefficient, ε_f' is the fatigue ductility coefficient, and b and c are exponents determined by experiments.

In order to include the mean stress effect on fatigue life, several models were proposed in literature. One method, often referred to as Morrow's mean stress method, replaces σ_f' by $\sigma_f' - \sigma_m$ in Eq. (5), where σ_m is the mean stress [18,35,36]:

$$\frac{\Delta\varepsilon}{2} = \varepsilon_a = \frac{\Delta\varepsilon_e}{2} + \frac{\Delta\varepsilon_p}{2} = \frac{\sigma_f' - \sigma_m}{E}(2N_f)^b + \varepsilon_f'(2N_f)^c \tag{6}$$

An alternative version of this model where both the elastic and plastic terms are affected by the mean stress is given by [35,37]

$$\frac{\Delta\varepsilon}{2} = \varepsilon_a = \frac{\Delta\varepsilon_e}{2} + \frac{\Delta\varepsilon_p}{2} = \frac{\sigma_f' - \sigma_m}{E}(2N_f)^b + \varepsilon_f'\left(\frac{\sigma_f' - \sigma_m}{\sigma_f'}\right)^{c/b}(2N_f)^c \tag{7}$$

In the case of multiaxial stress and strain states, the equivalent alternating strain can be used [35,36,38] in Eq. (7) assuming proportional loading using either the maximum principal strain,

$$\varepsilon_{qa} = \varepsilon_{a1} \tag{8}$$

the maximum shear strain,

$$\varepsilon_{qa} = \frac{\varepsilon_{a1} - \varepsilon_{a3}}{1 + \nu} \tag{9}$$

or the octahedral shear strain,

$$\varepsilon_{qa} = \frac{\sqrt{(\varepsilon_{a1} - \varepsilon_{a2})^2 + (\varepsilon_{a2} - \varepsilon_{a3})^2 + (\varepsilon_{a3} - \varepsilon_{a1})^2}}{\sqrt{2}(1 + \nu)} \tag{10}$$

where ε_{a1}, ε_{a2}, and ε_{a3} are principal alternating strains with $\varepsilon_{a1} > \varepsilon_{a2} > \varepsilon_{a3}$.

Another equation suggested by Smith, Watson, and Topper (often called the "SWT parameter") is given by [30,35,37]

$$\sigma_{\max}\varepsilon_a E = (\sigma_f')^2(2N_f)^{2b} + \sigma_f'\varepsilon_f' E(2N_f)^{b+c} \tag{11}$$

In order to save time and cost, it is often desirable to estimate fatigue life of a component or structure with a reasonable degree of accuracy using easily and quickly obtainable material properties such as hardness and tensile strength. Accordingly, many universally valid correlations between monotonic strength data and fatigue life have been proposed in literature based on experimental data [30,35]. Among these relations, the modified universal slopes method proposed by Muralidharan and Manson is the best known and is given by [30,35,37]

$$\frac{\Delta\varepsilon}{2} = \varepsilon_a = 0.623\left(\frac{S_{\text{ut}}}{E}\right)^{0.832}(2N_f)^{-0.09} + 0.0196(\varepsilon_f)^{0.155}\left(\frac{S_{\text{ut}}}{E}\right)^{-0.53}(2N_f)^{-0.56} \tag{12}$$

where S_{ut} is the ultimate tensile strength. Another universal relation based on Brinell hardness [30] is given by

$$\frac{\Delta\varepsilon}{2} = \frac{4.25(HB) + 225}{E}(2N_f)^{-0.09} + \frac{0.32(HB)^2 - 487(HB) + 191{,}000}{E}(2N_f)^{-0.56} \tag{13}$$

The final two approximations do not require coefficients or exponents specific to a material. They use only hardness, ultimate tensile strength, and modulus of elasticity (in megapascals) for strain-life calculations; all of which are commonly available or easily measurable. These equations are applicable to a range of materials.

Downloaded 26 Dec 2008 to 193.140.210.85. Redistribution subject to ASME license or copyright; see http://www.asme.org/terms/Terms_Use.cfm

Table 1 Mechanical properties of St 12 03 (DIN 1623) steel

No. of tests performed	4
Average tensile strength (MPa)	319.64 (2.43[a])
Average yield strength (MPa)	217.41 (1.25[a])
Average reduction in area (%)	35.59 (2.71[a])
Average hardness for base metal (kgf/mm^2)	105.5
Average hardness for HAZ (kgf/mm^2)	106.2
Average hardness for nugget (kgf/mm^2)	112.6

[a]The values inside the parentheses show standard deviations of the values.

3 Experimental Study

3.1 Material. In this study, fatigue failure tests were carried out on MTS specimens made of a low carbon cold rolled steel, St 12 03 (DIN 1623). The average mechanical properties and the chemical composition of St 12 03 are given in Tables 1 and 2, respectively. Materials of this type are widely used in automotive industry, especially to construct body frames. Low carbon steels are cheaper and easier to process in comparison to high carbon steels. Although they have lower fatigue strength, they are less sensitive to notches and surface imperfections. Also, they weld evenly and easily and hold paint well.

A spot-welded joint is composed of a nugget and base metal. Because elastic modulus and Poisson's ratio are not affected by heat treatment, their magnitudes remain the same throughout the specimen (E=207 GPa and ν=0.25) despite melting during the formation of the nugget. Although the nonlinear stress-strain relation of the material in and around the nugget was affected during the joining operation, this effect was neglected considering that the steel was not a hardened steel. In Table 1, the results of microhardness tests on base metal, heat affected zone (HAZ), and nugget are given. Because the hardness levels at these locations are close to each other, one may assume that there is no significant change in mechanical properties of the material during welding. The engineering stress-strain curve of the base material (DIN 1623), shown in Fig. 1, was assumed to be valid for the nugget and HAZ.

3.2 Specimens. The specimens tested in this study are made of three strips of steel sheets joined by spot welds, as shown in Fig. 2. Unlike TS specimens, MTS specimens contain plates bent at their sides. This increases the flexural rigidity and thus resistance to bending and buckling. In our case, the central plate was bent and joined to two flat plates through two resistance spot welds. The shaded regions indicate the gripped portions of the specimen during testing.

Table 2 Chemical composition of St 12 03 (DIN 1623) steel

Element	C	Mn	P	S	Si	Al
% weight	0.0675	0.21	0.008	0.008	0.01	0.06

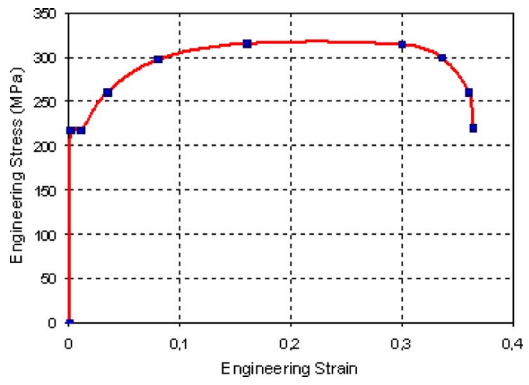

Fig. 1 Engineering stress-strain curve

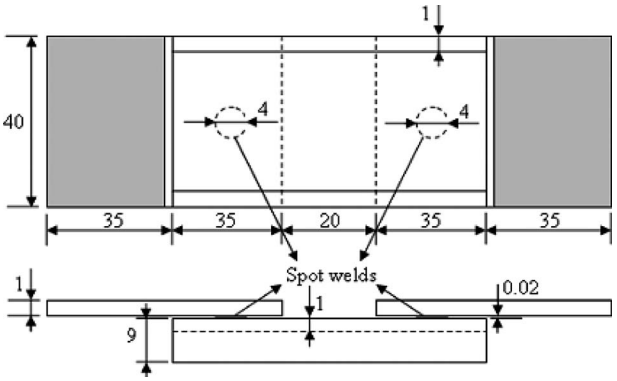

Fig. 2 Geometry of the MTS specimens

There are various industry standards for sizing a spot weld for a given sheet metal thickness. For instance, the American Welding Society (AWS), Society of Automotive Engineering (SAE), and the American National Standards Institute (ANSI) together recommend a weld nugget diameter for steels [5] given by

$$d \approx 4\sqrt{t} \tag{14}$$

where d and t are the weld nugget diameter and sheet thickness, respectively (in millimeters). This recommended formula is empirical in nature obtained through extensive experiments. Interestingly, this formula is valid independent of the varying properties of the materials [5,39]. In this study, the specimens were made of a metal sheet having 1 mm thickness. In accordance with the formula, the spot-weld nugget diameter was selected as 4 mm. Welding parameters are given in Table 3. In order to realize the desired nugget diameter, the joining operation was repeated using a number of different values for the welding parameters, and the set of values leading to the desired diameters was chosen. Several peel tests were also performed during the fabrication of the specimens in order to ensure that the weld nugget size did not change due to tip wear.

All pieces of MTS specimens were sheared from steel sheets. The blanks were cut in a way that the loading direction of the final specimen was parallel to the steel rolling direction. After the three pieces of the specimen were machined, they were prepared for the welding process. Each one of the three pieces was rinsed in methyl alcohol and then dried in order to remove the oil coating to avoid its adverse effect on welding. In automated (or standard) type of spot welding process, two electrodes clamp the two sheets of metal together with a considerable force while transmitting current. A manual type of spot welding process, on the other hand, is achieved just by touching the electrode on one surface of the specimen without applying a clamping force. An electrode force of a few kgf is sufficient to achieve contact between the metal sheets.

3.3 Test Equipment and Testing. The fatigue tests were performed in air at room temperature on a Material Testing System (MTS) with 100 kN capacity, which had a closed loop servohy-

Table 3 Welding parameters for the spot-weld joints

Spot-weld type	Manual spot	Automated spot
Electrode force (kgf)	—	150
Welding current (A)	14	10
Weld time (cycles at 60–80 Hz)	7.5	8.5
Electrode diameter (mm)	4.45	4.45

Downloaded 26 Dec 2008 to 193.140.210.85. Redistribution subject to ASME license or copyright; see http://www.asme.org/terms/Terms_Use.cfm

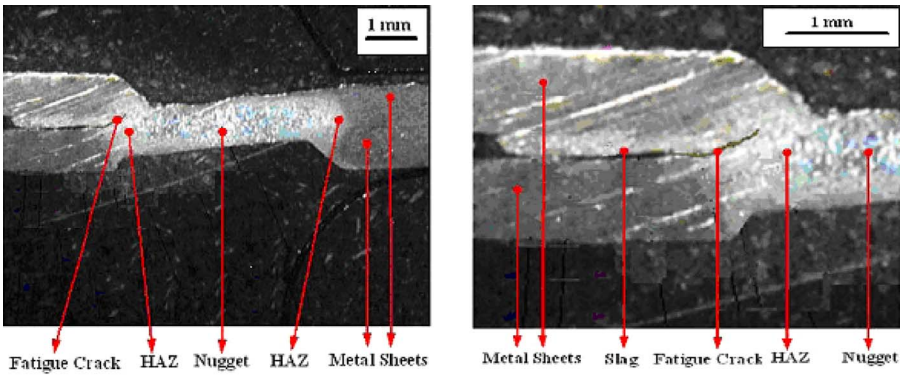

Fig. 3 Cracks in a tested and deformed automated-type spot weld: (*a*) larger view and (*b*) focused on the left region

draulic testing system with a digital controller. Hydraulically operated grips using universal tapered collets were used in order to secure the specimen ends in series with the load cell. Special attention was given to align the load train; that is, the load cell, grips, specimen, and actuator. The specimens were mounted in the grips 30 mm from both ends. The loading direction in both tensile and fatigue tests was the same as the rolling direction of the cold rolled sheets.

In automotive applications, a load cycle with an R-ratio ($R = P_{\min}/P_{\max}$) between 0.01 and 0.1 is commonly used [40]. Accordingly in the fatigue tests, a constant-amplitude sinusoidal load was applied with an R-ratio between 0.04 and 0.08. In total, ten different load ranges for automated and manual types of spot welds were applied to determine the failure modes and the fatigue life of the specimens. Tests were repeated using two or three specimens for each load case. If the discrepancy in the fatigue lives of two specimens tested under the same load range was greater than 10%, the test was repeated. Due to time constraints, tests involving long fatigue lives (greater than 500,000 cycles) were conducted only once; but the fatigue life-load trend was observed to be maintained also for the low loads. The tests were performed with an operating frequency in the range of 1–5 Hz. In this study, frequency of loading was assumed not to affect the fatigue life at low frequencies (below 10 Hz) as the previous studies indicated [18].

3.4 Observations on Fatigue Crack Development. The cracks propagating through the thickness of the sheet and leading to fracture were identified as the primary cracks and the corresponding weld as the primary weld. The primary cracks were always observed to occur in the flanged piece (the central plate) of the MTS specimens on their inner surfaces. The flat portions, on the other hand, might contain secondary cracks, which could not propagate through the sheet thickness. All of the tested and ten of the untested specimens were cut and embedded in epoxy resin, then polished and etched for macro-inspection. After etching, the HAZ and nugget areas were examined under an optical microscope (Figs. 3–6). In Fig. 3, a crack can be seen to develop at the periphery of the nugget. After cracks initiated and grew, localized necking in the base metal some distance away from the nugget boundary (in other words in the HAZ) occurred, and finally the specimens were torn apart. During the formation of an automated weld, some of the molten metal was squeezed out of the nugget region into the interface between the sheets due to electrode force. This is shown as expulsion in Figs. 3 and 4.

In manual welds, a small crater develops on the side of the plates on which the electrode touches, as shown in Figs. 5 and 6, even though the applied force is small in comparison to 150 kgf clamping force used in automated welds. This occurs because a larger current is applied to form manual welds, which generates a larger amount of heat and melting.

Although in some cases (one out of three specimens) gaps or porosities were observed inside the manually formed nuggets in tested and untested specimens (Fig. 6), cracks always occurred on the peripheries of the spots, not in the nuggets. Therefore, the load bearing capability of a spot-welded joint may not be significantly reduced by the existence of voids in the central region of the nugget. Previous studies also showed that neither nugget porosity,

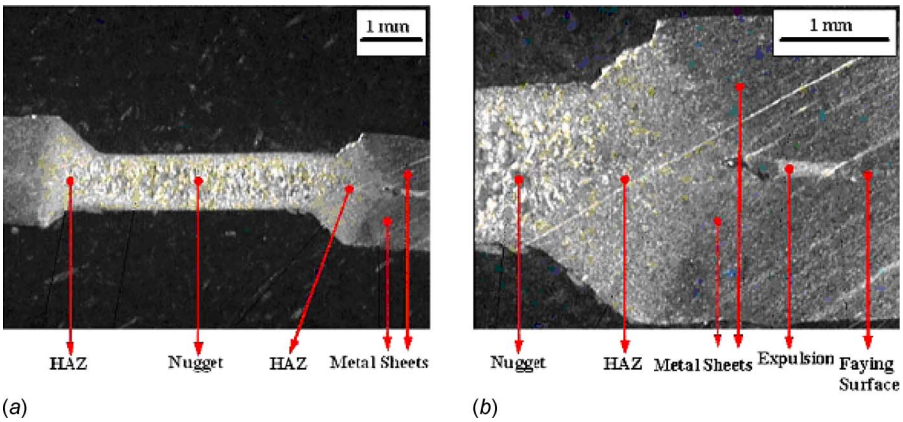

Fig. 4 An automated-type spot weld in an untested MTS specimen: (*a*) larger view and (*b*) focused on the right region

Downloaded 26 Dec 2008 to 193.140.210.85. Redistribution subject to ASME license or copyright; see http://www.asme.org/terms/Terms_Use.cfm

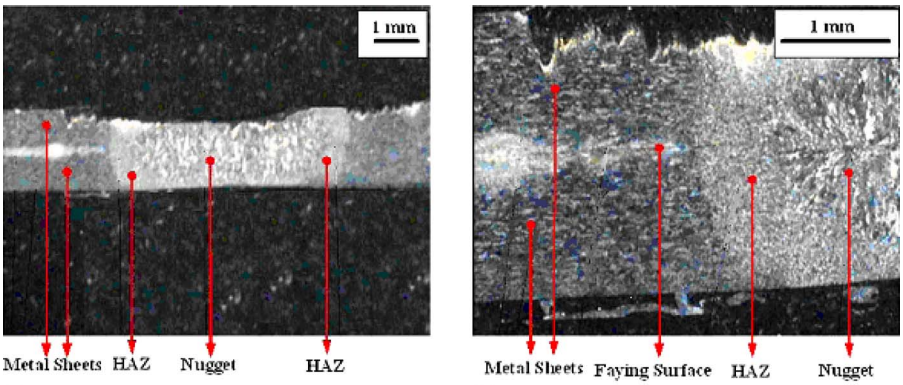

Fig. 5 A manual-type spot weld in an untested MTS specimen: (*a*) larger view and (*b*) focused on the right region

up to about 40% of the weld diameter, nor deep surface indentations had major impacts on the fatigue behavior of the welds [41].

3.4.1 Failure Modes. There are various failure modes for spot welds. First of all, although rarely observed, interfacial failure may occur due to a fracture parallel to the sheets. This type of failure is called a "weld-interface-failure mode" (Type-1, as shown in Fig. 7) [23]. Yielding across the nugget may occur due to poor welding or very small nugget size. In most cases, however, spot welds fail due to through thickness fatigue cracks [20,41] as observed in this study. A fatigue crack initiates in a highly stressed region near the nugget. Once a crack develops, one of two things may happen. If the load is sufficiently small, the crack initiates at some distance away from the nugget and then propagates around the nugget to a large width before propagating through the thickness. This type of failure mode is called "the sheet tearing mode through width" (Type-2A). However, if the load is sufficiently high, the crack initiates closer to the nugget and propagates through the thickness without becoming wide. This is called "the sheet tearing mode through thickness" (Type-2B) [19]. In this second type of failure mode, the crack grows into a semi-elliptical shape and then propagates through the sheet thickness and finally the sheets separate from each other. Lastly, sometimes the weld is pulled out of one of the sheets. This type of failure mode is called as "the nugget pull-out mode" (Type-3) [34]. All these failure modes are depicted in Fig. 7. In the 40 tests conducted in this study, the number of instances each failure mode is observed is given in Table 4.

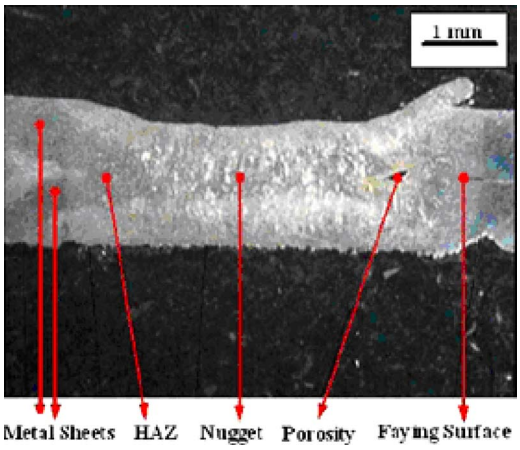

Fig. 6 Porosity in a manual spot-welded MTS specimen

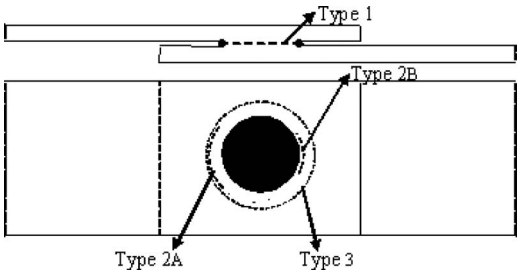

Fig. 7 Depiction of the failure modes observed in the spot-welded MTS specimens

The sheet tearing mode through thickness (Type-2B) is very common for MTS specimens for the chosen load ranges. In this type of failure mode, the first crack that propagates through the thickness of the sheet is defined as the primary crack and the corresponding weld is defined as the primary weld. The crack on the opposite side of the primary weld is called the secondary weld, which also has its own primary and secondary cracks [18,21], as shown in Fig. 8. Figure 9 shows the load transfer path in the spot-weld specimen. Cracks nucleate at the gap between the plates on the faying surfaces near the spot weld and then propagate through the thickness.

3.4.2 Fatigue Lives. As in the previous studies [18,20,35], the fatigue life was defined as the number of loading cycles it takes for the first crack to initiate and propagate through thickness of the sheet and become visible from the outer side of the sheet. In that case, testing of the specimen was immediately terminated. After a through crack had appeared, the maximum deflection increased quickly, indicating a significant decrease in the stiffness of the specimen. In order to aid in the visual detection of a crack, a small amount of machine oil was deposited between the specimen sheets before testing. When the crack grew through the sheet, it allowed the oil to seep through and appear on the outer surface of the sheet signaling failure.

Table 5 shows the tabulated data of the applied load ranges (P_{min}, P_{max}) and the corresponding experimental fatigue lives of the specimens. Manual-type spot-weld joints endured 30–45% shorter life in comparison to automated-type spot-weld joints. Although sometimes porosities were observed in the manual spots (Fig. 6), the nugget did not fail. On the contrary, cracks leading to

Table 4 Distribution of the failure modes observed in the specimens

Failure mode	Type-1	Type-2A	Type-2B	Type-3
No. of tests	1	4	32	3

Downloaded 26 Dec 2008 to 193.140.210.85. Redistribution subject to ASME license or copyright; see http://www.asme.org/terms/Terms_Use.cfm

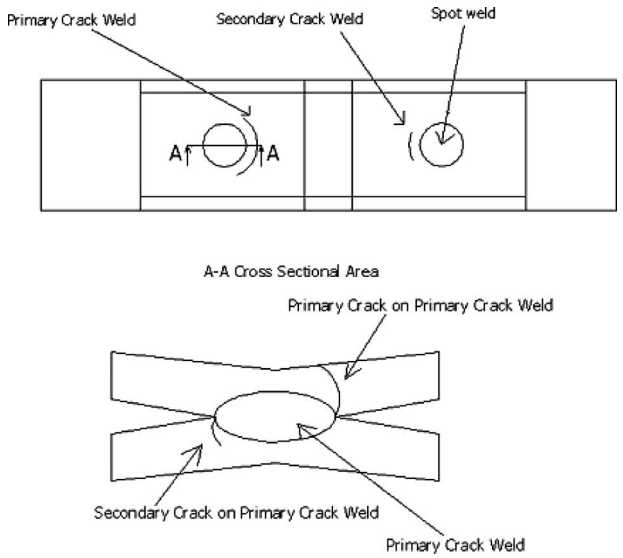

Fig. 8 Typical failure mode (Type-2B) for MTS specimens

fatigue fracture appeared close to the nugget edges and propagated through the thickness as in the automated welds. The reason why the manual spots are weaker to fatigue loading may be attributed to higher stress concentration arising from nonsymmetric weld geometry and sharper edges.

4 Statistical Analysis of the Experimental Data

The scatter in fatigue lives is large even under controllable and repeatable testing conditions. Imprecision in testing equipment, loose tolerances in specimen dimensions, large variations in environmental conditions, etc., may lead to unacceptably large scatter in data. For this reason, one should ensure that the scatter in experimental data is within the acceptable range, and tests are conducted under controllable and repeatable conditions. This requires a statistical analysis of the data. One of the ways to estimate the scatter in fatigue life is to calculate the coefficient of variation (COV). The typical values of COV for mild steels range from 0.10 in low cycle fatigue to 0.5 in high cycle fatigue [42,43]. High strength materials seem to exhibit larger scatter in fatigue life [43]. The COV values for welded joints are even higher [44]. Tables 6 and 7 show COV values of fatigue lives of spot-weld joints corresponding to the load ranges indicated in Table 5. As seen in these tables, the fatigue life data experimentally obtained in this study have lower values of COV than the typical ones for all loading cases. This shows that the data are reliable and the testing conditions are repeatable and controllable. Variations in the data are then mostly attributable to the inherent characteristics of the material not to the testing conditions. One should also note that the values of COV for automated-type spot welds being somewhat lower imply that this type of specimens is more repeatable.

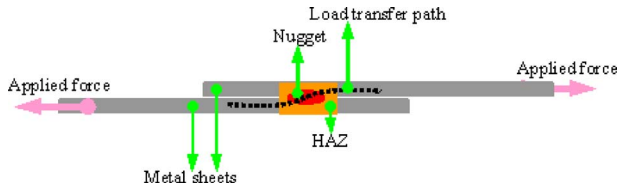

Fig. 9 The load transfer path for the MTS specimens under loading

Table 5 Fatigue lives of the specimens and the number of samples tested, *n*

Manual-type spot				Automated-type spot			
P_{max} (N)	P_{min} (N)	n	N_f (cycles)	P_{max} (N)	P_{min} (N)	n	N_f (cycles)
3700	200	5	9970	3700	200	5	13,370
3000	150	4	39,000	3000	150	4	61,190
2700	150	4	52,470	2700	150	4	93,480
2400	150	3	93,550	2400	150	3	167,100
2200	150	3	163,546	2250	150	2	283,150
2100	150	2	433,452	2150	100	1	633,250

Table 6 Mean, standard deviation, and COV values for the automated-type spot welds

Automated-type spot weld			
Life range	Mean value	Standard deviation	COV
13,280–13,450	13,370	80.932	0.006
58,660–62,970	61,190	1851.4	0.030
90,750–95,000	93,480	1875.26	0.020
159,250–172,300	167,100	6916.83	0.041
265,700–300,600	283,150	24,678.03	0.087
633,250	633,250	N/A	N/A

Table 7 Mean, standard deviation, and COV values for the manual-type spot welds

Manual-type spot weld			
Life range	Mean value	Standard deviation	COV
9800–10,100	9970	132.85	0.013
36,500–41,500	39,000	2198.48	0.056
49,000–55,940	52,470	3270.16	0.062
79,650–102,450	93,550	12,194.67	0.130
143,456–185,432	163,546	21,045.55	0.129
416,474–450,430	433,452	24,010.52	0.055

In order to judge whether the scatter is within the acceptable range, one may also examine the regression coefficients obtained through a regression analysis of the experimental data. It is known that fatigue life data can typically be fitted to a power-law. Figure 10 shows the experimental data points and the fitted lines with their respective coefficient of determination (R^2) values for the manual-type and automated-type spot welds. The value of R^2 being close to 1.0 indicates that the linear line is a good fit for the data, and the predictability of the regression is quite high.

Tables 8 and 9 show the 95% and 99% confidence intervals of the mean for automated-type and manual-type spot-welded specimens, respectively.

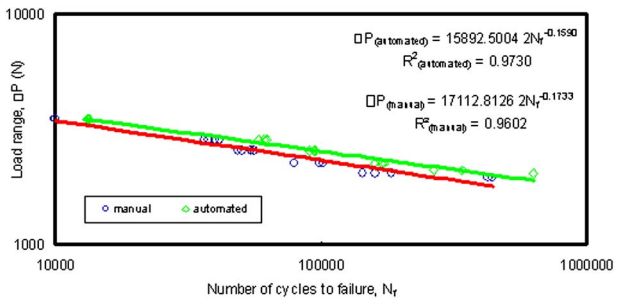

Fig. 10 The resulting curve of the regression analysis for both the manual-type and the automated-type spot welds

Downloaded 26 Dec 2008 to 193.140.210.85. Redistribution subject to ASME license or copyright; see http://www.asme.org/terms/Terms_Use.cfm

Table 8 The confidence interval of the mean for automated-type spot-welded specimens

The confidence interval for the mean for the automated-type spot weld			
For the 95% interval		For the 99% interval	
13,299	13,441	13,277	13,463
59,376	63,004	58,802	63,578
91,642	95,318	91,061	95,899
159,273	174,927	156,797	177,403
248,948	317,352	238,129	328,171
N/A	N/A	N/A	N/A

Table 9 The confidence interval of the mean for manual-type spot-welded specimens

The confidence interval for the mean for the manual-type spot weld			
For the 95% interval		For the 99% interval	
9854	10,086	9817	10,123
36,845	41,155	36,164	41,836
49,265	55,675	48,250	56,688
79,750	107,350	75,385	111,715
139,731	187,361	132,197	194,895
400,175	466,729	389,649	477,255

5 Finite Element Model

Fatigue life prediction models require accurate calculation of stress and strain states developed in the structure. For this purpose, commercial FEA software, ANSYS (version 10), was used. Residual stresses developed during the formation of the spot weld were assumed not to affect the fatigue life and were not considered in the stress analysis. However, the residual stresses arising from nonuniform plastic deformations were determined through the nonlinear stress analysis. Dynamic effects were neglected, and the load was assumed to be applied quasistatically.

The actual behavior of the material may exhibit a combination of isotropic hardening and kinematic hardening characteristics. Assumption of purely isotropic hardening may lead to nonconservative predictions. In the absence of full characterization of the material, a kinematic hardening material model (KINH) was considered to be more appropriate to simulate the nonlinear deformation behavior. This model uses the Besseling formulation [35,36,45], which includes the Bauschinger effect in cyclic loading. The data points were taken from the true stress-strain diagram, which was obtained by converting the engineering stress-strain diagram shown in Fig. 1.

In the FE model, a 3D ten-node tetrahedral solid element, SOLID92, was used for the sheet metal. This element has plasticity, stress stiffening, large deflection, and large strain capabilities. Several types of models have been proposed in literature for spot-weld nuggets: single-bar model [12], spoke-bar model [12,28], multiple rigid-bar model [7,12], and solid nugget model [6,8,12,17,18,34,46]. Modeling the beam using solid elements leads to difficulties in meshing because this requires matching of the meshes of different parts. Besides, since the length of the nugget is equal to the gap between the plates, which is very small, tiny solid elements should be generated for the nugget. This adds enormously to the computational time. For these reasons, a different approach was adopted in this study; the nugget was modeled using a two-node beam element, BEAM188. Contact and target elements, Targe170 and Conta175, were created on the inner surfaces around the spots. The beam element, BEAM188, is based on Timoshenko beam theory. Shear deformation effects are, therefore, included, which are especially important for short beams. This element has six degrees of freedom at each node. The beam shares a single node on each plate. One should note that solid elements that are used to model the plates do not have rotational degrees of freedom unlike the beam element used for the nugget. In order to prevent relative rotation of plates with respect to spot weld at the connection points, the nodes on the plates that lie within the region of the spot-weld radius are constrained to move within the plane perpendicular to the beam. Because the nugget experiences low stresses as reported in previous studies [21], its material model was chosen as linearly elastic.

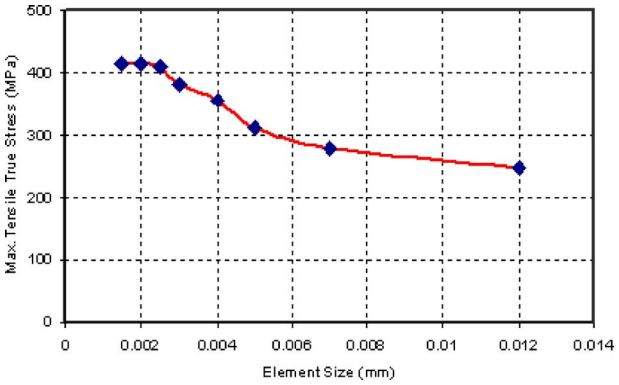

Fig. 11 Convergence in terms of element size

In order to obtain an appropriate mesh structure that may enable accurate calculation of the stress state, a convergence analysis was carried out for the element size. In the FE analysis, a load range of 2700–150 N was applied. Figure 11 shows the maximum tensile stress calculated using different element sizes. Convergence was obtained for 0.002 mm element size. The size of the elements used within and around the spot-weld nugget was chosen to be much smaller than 0.002 mm to correctly determine the stress state in this highly stress region. Figure 12 shows the finite element mesh. Figure 13 depicts a detail of the mesh on the section passing through the middle of the right spot weld.

In ANSYS, a load step is applied in increments with a certain number of substeps. A convergence analysis was also performed to determine the number of substeps necessary for accuracy. As shown in Fig. 14, 160 substeps are adequate for an accurate analysis.

Because the automated-type spot weld was formed by pressing the plates at both sides, some of the molten material is squeezed out into the interface between the plates. As seen in Fig. 3, the extent of the expelled material accumulated between the plates may reach up to 15–20% of the sheet thickness. Accordingly, the space or gap between the overlapping portions of the plates was taken as 0.2 mm. Because different values were suggested in literature (e.g., 0.02 mm in Ref. [47]), the effect of the extent of the gap on fatigue life was also investigated.

5.1 Boundary Conditions. The boundary conditions of the FE model, as shown in Fig. 15, were chosen so that they could realistically reflect the conditions of the fatigue experiments. The x axis shows the loading direction and the z axis shows the out-of-plane direction. The two ends of the specimen were hold by

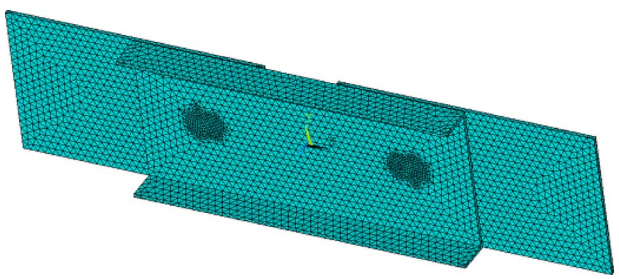

Fig. 12 Finite element model for the MTS specimen

Downloaded 26 Dec 2008 to 193.140.210.85. Redistribution subject to ASME license or copyright; see http://www.asme.org/terms/Terms_Use.cfm

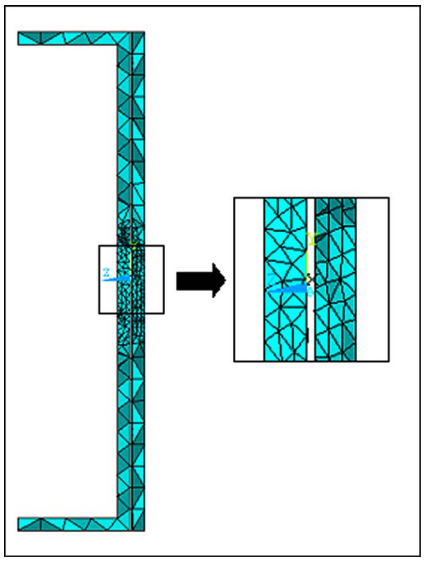

Fig. 13 A detail of the mesh at and around the right spot weld of the specimen

grips, one being stationary, and the other applying the load. Accordingly, in the FE model, all displacements and rotations were restrained at one end and uniform pressure was applied along the x direction at the other end while the other degrees of freedom were restrained.

5.2 Resulting Stress States. The cyclic loading was applied in two load steps. First, the load was incrementally increased to its maximum value, F_{max}, and the resulting stress state was obtained. In the second load step, the load was incrementally decreased to its minimum value, F_{min}. Stress saturation was assumed to be achieved in the first cycle such that in the next load cycles, stresses were to fluctuate between the minimum and maximum stress levels calculated for the first load cycle. Strain hardening, strain softening, or mean stress relaxation effects commonly observed in cyclic loading were assumed not to have significant influence on fatigue life.

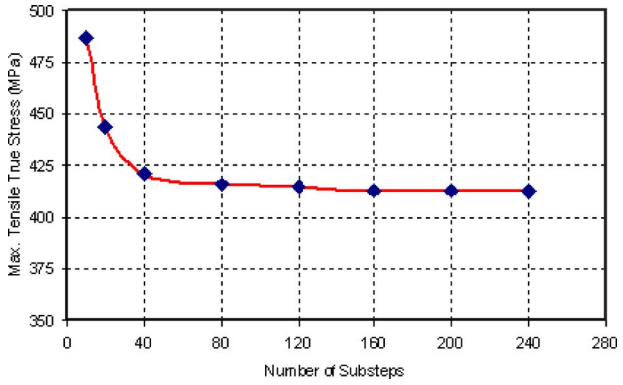

Fig. 14 Convergence in terms of substeps

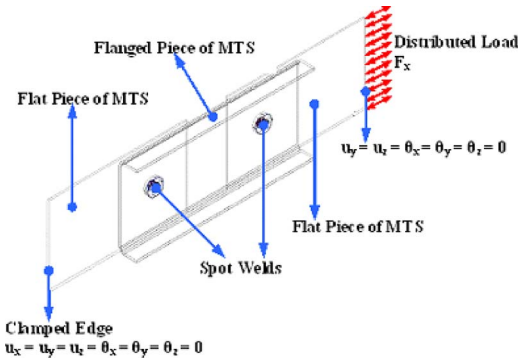

Fig. 15 Boundary conditions of the finite element model

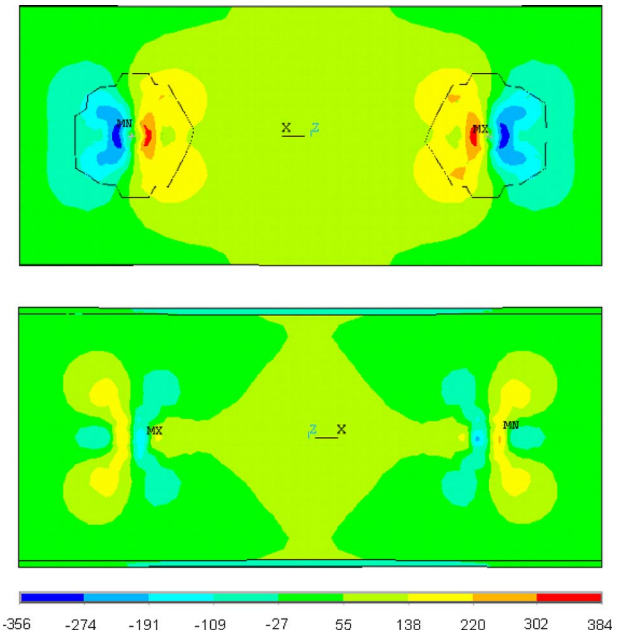

Fig. 16 The distribution of the σ_{xx} component (in megapascals) of stress on the inner (upper figure) and outer (lower figure) surfaces of the central plate developed due to maximum load (2700 N)

Figures 16 and 17 show the distributions of the σ_{xx} component of stress on the inner and outer surfaces of the central plate de-

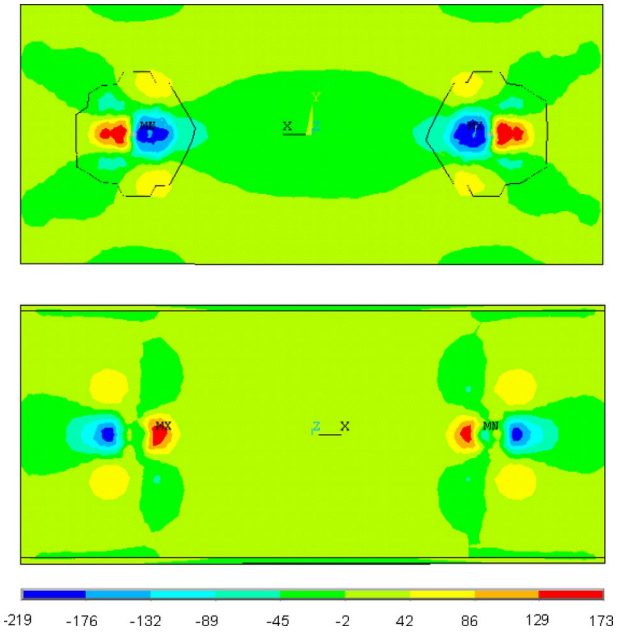

Fig. 17 The distribution of the σ_{xx} component (in megapascals) of stress on the inner (upper figure) and outer (lower figure) surfaces of the central plate developed due to minimum load (150 N)

Downloaded 26 Dec 2008 to 193.140.210.85. Redistribution subject to ASME license or copyright; see http://www.asme.org/terms/Terms_Use.cfm

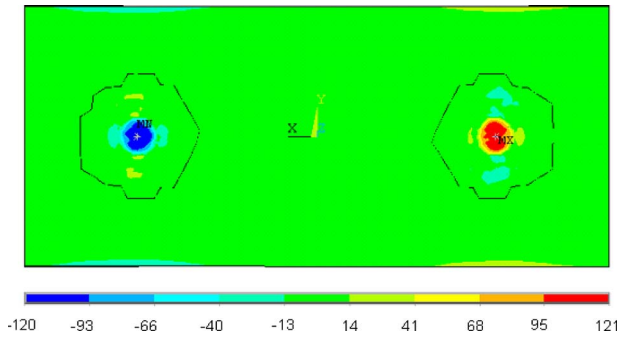

Fig. 18 The distribution of the τ_{xz} component (in megapascals) of stress on the inner surface of the central plate developed due to maximum load (2700 N)

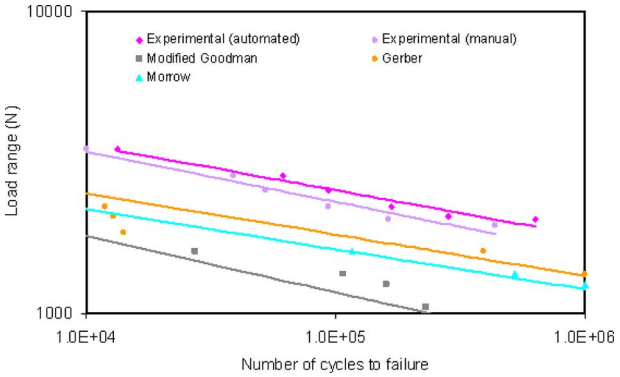

Fig. 19 Comparison of the fatigue lives predicted using stress-based approaches and experimental results

veloped after the maximum (2700 N) and minimum (150 N) loads are applied, respectively. High stresses develop at regions on the inner surfaces of the sheets close to the peripheries of the spot-weld nuggets. Since the minimum load is tensile and quite low (150 N), significant compressive stresses existing after unloading may only be attributed to residual stresses developed due to nonuniform plastic deformation. Although load transfer occurs through the spot-weld joint, the nugget is subject to low stresses since its thickness is large in comparison to the sheet thickness. Besides, the nugget is mainly subject to shear loading, as seen in Fig. 18, and the plate is mainly subject to a bending moment. Unsurprisingly, bending induces larger stresses. Due to the effect of bending, stresses change from tension to compression through the thickness, as seen in Fig. 16. The peak tensile stress develops close to the spot weld but not on its circumference. This location also conforms to the fatigue crack initiating sites observed in the experiments.

When the location of the point where the maximum tensile stress developed was examined, this point was observed to become closer to the nugget boundary with the decreasing load range. For the cases with maximum loads of 2700 N, 1750 N, and 750 N, the distances of the critical point to the nugget circumference were 0.42 mm, 0.39 mm, and 0.35 mm, respectively. This conformed to the trend that crack initiation sites were closer to the nugget for low loads as observed in the experiments. The reason why the maximum stress develops at a farther distance from the nugget with a larger load may be attributed to an enlarged yield zone away from the nugget.

6 Estimated Fatigue Lives

6.1 Calculation of Fatigue Lives. The process of nucleation, growth, and joining of microcracks is expected to take place in highly stressed regions. Fatigue crack growth is known to occur along planes where the tensile stress takes its maximum value. Hence, the fatigue life calculations were carried out using the stress and strain states in the element at which the maximum tensile stress develops for the given maximum loading case. This element is located at the faying surface or HAZ around the peripheries of the spot welds, as indicated in Fig. 16. The fatigue properties of the material used in the fatigue assessment models are given in Table 10 [35].

Table 10 Fatigue data of the material used in the fatigue assessment models

σ_f' (MPa)	σ_f (MPa)	ε_f'	ε_f	b	c	HB
499	475	0.104	1.63	−0.06	−0.4	105.1

6.2 Comparison of the Predicted and Measured Fatigue Lives. The fatigue lives of the specimens were estimated using the available fatigue assessment models. Figure 19 shows the load range versus the number of cycles to failure obtained through the experiments and fatigue analyses. The fatigue lives given in the figure were predicted using the stress-based approaches. The lines shown in the figure are fitted to the data. It should be noted that Fig. 19 contains off-data; that means some of the data are outside the range shown in the figure. The best correlations were obtained via Gerber's and Morrow's models. Nevertheless, their predictions were overly conservative for spot-weld joints. This may be because these models do not adequately account for the effects of the highly localized plastic deformation around the spot-weld nuggets.

Figure 20 shows a comparison of the experimentally determined fatigue lives and the predictions based on the strain-based approaches. Coffin–Manson and Morrow's mean stress models yielded the best correlation. Considering the scatter in the data, the agreement with the experimental results was excellent for both low and high cycle fatigue. The models, especially Coffin–Manson, captured the increasing trend of fatigue life with decreasing load. Its predictions are close to the 99% confidence interval of the manual spot-weld data given in Table 9. All of the models predicted a life greater than 1×10^6 cycles for a maximum load of 1750 N. The fact that a better correlation was obtained via Coffin–Manson model, which does not take into account the effect of mean stress, in comparison to Morrow's mean stress model implies that the influence of mean stress on fatigue life of spot welds is not significant in spot-weld joints. This may be because plastic strains were not large. The maximum principal strains for the maximum and minimum peak loads of 3700 N and 2100 N were calculated as 0.107 and 0.028, respectively. No observed effect of

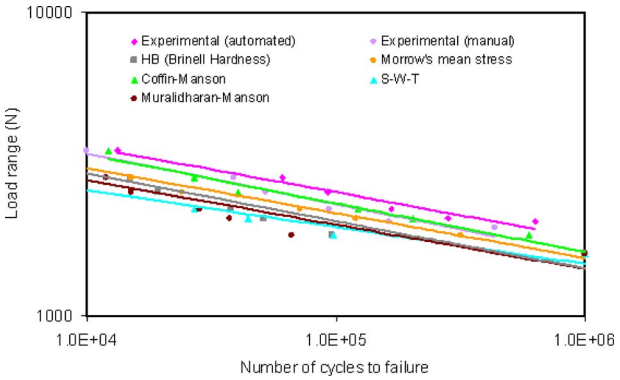

Fig. 20 Comparison of the fatigue lives predicted using strain-based approaches and the experimental results

Downloaded 26 Dec 2008 to 193.140.210.85. Redistribution subject to ASME license or copyright; see http://www.asme.org/terms/Terms_Use.cfm

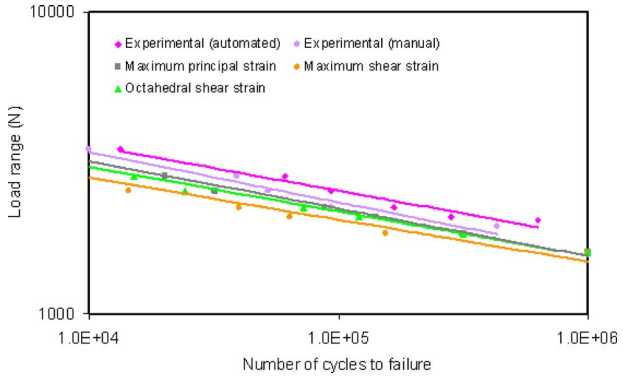

Fig. 21 Comparison of the fatigue lives predicted using Morrow's mean stress model with different equivalent strain approaches

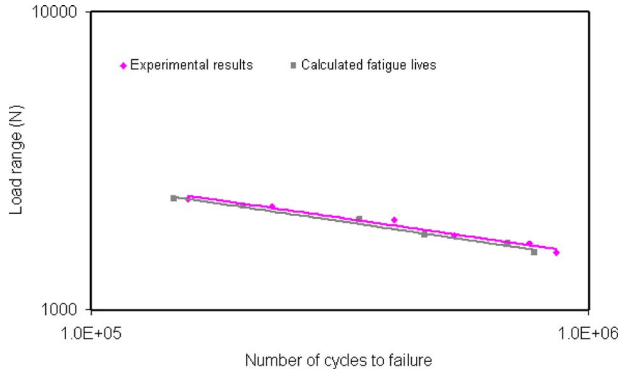

Fig. 23 Comparison of the fatigue lives obtained experimentally by Pan and Sheppard [17] and Pan [18] and predicted using Morrow's mean stress approach

mean stress also corroborates our assumption that residual stresses developed during the welding process have little effect on fatigue life since they mainly affect mean stress rather alternating stress. Accurate and consistent predictions of the model for spot-weld joints in which highly complex stress states develop imply that the model adequately reflects the effects of the basic underlying mechanisms leading to fatigue failure for typical engineering applications.

In order to apply the models, which account for fatigue failure only in uniaxially loaded parts, we need to find equivalent stress and strain values representing the multiaxial stress and strain states that developed in the spot-weld joint. There are mainly three approaches: the maximum principal strain (Eq. (1)), the maximum shear strain (Eq. (2)), and the octahedral shear strain (Eq. (3)). Figure 21 shows the fatigue lives predicted by Morrow's mean stress method using different equivalent strain approaches. As seen in the figure, the octahedral shear strain and the maximum principal strain better represent the effect of multiaxial strain state.

As mentioned earlier, the fatigue lives were calculated based on the stress and strain states at the point where the maximum tensile stress developed. Alternatively, the points where the maximum shear stress or von Mises stress developed were also tried. However, nonconservative predictions were obtained for high cycle fatigue. Thus, the criterion initially adopted to determine the critical point turned out to be appropriate.

The gap between the overlapping portions of the MTS specimen depends on a number of factors: gripping force, intensity of welding current, sheet thickness, etc. This in turn affects the resulting stress state. Figure 22 shows the predicted effect of the gap on fatigue life. Understandably, the larger the gap, the larger the stresses and the shorter the fatigue life since increased distance between the plates leads to larger bending moments.

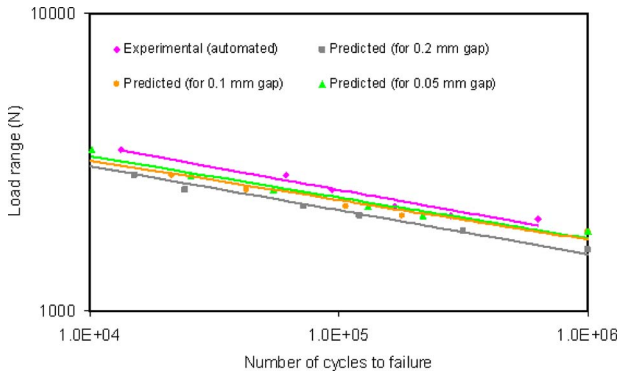

Fig. 22 Comparison of the fatigue lives predicted for different gap values using Morrow's mean stress approach and experimental results

The numerical part of this study was also verified by comparing the predictions of the models with the fatigue lives of the automated-type spot-welded MTS specimens experimentally obtained by Pan and Sheppard [17] and Pan [18]. The same finite element modeling was used to analyze the specimens using the material properties, loading, and geometry of the specimens provided in that study. Fatigue lives were predicted using Morrow's mean stress approach. As seen in Fig. 23 the results compare quite well. One should also note that better correlation obtained with the data provided by Pan and Sheppard [17] and Pan [18] in comparison to the data obtained in the present study may be attributed to the use of the material properties of the HAZ in the FE calculations for the former case rather than the properties of the base metal.

7 Conclusions

In this study, the fatigue failure behavior of modified tensile-shear specimens was investigated both experimentally and numerically. Fatigue tests were conducted applying various load ranges on specimens. Two different types of spot-weld joints, automated and manual, were tested, and load range-fatigue life curves were obtained. Crack development and deformation patterns were identified. Experimental results showed that the number of cycles to failure for manual-type spot-welded specimens was 30–45% lower than that of the automated-type joints. Examination of deformed and undeformed specimens under an optical microscope revealed the existence of some gaps or porosities in the manual-type spot-weld nuggets; but cracks leading to fatigue fracture always occurred on the peripheries of the nuggets on the inner surfaces of the plates as in the automated-type weld joints. The difference might be due to stress concentrations arising from unsymmetric weld geometry.

FE analyses were carried out taking into account nonlinear constitutive relations, plastic deformation, and residual stresses to determine the stress and strain states in the specimens under cyclic loading. High stresses were found to develop close to the spots on the inner surfaces of the plates, which conformed to the fatigue crack initiation sites observed in the experiments.

The fatigue lives of the specimens were also estimated using the available general purpose fatigue failure models. Because the stress state in the spot-weld specimens was multiaxial and the fatigue models were structured for uniaxially stressed parts, equivalent stress or strain approaches were adopted. Among them, von Mises stress and maximum principal strain (or octahedral shear strain) were found to better reflect the effect of multiaxial strain and stress states. Both stress- and strain-based approaches were used to estimate the number of cycles to failure. The fatigue

Downloaded 26 Dec 2008 to 193.140.210.85. Redistribution subject to ASME license or copyright; see http://www.asme.org/terms/Terms_Use.cfm

life predictions of stress-based approaches were overly conservative. Among the strain-based approaches, Coffin–Manson and Morrow's means stress models yielded the best correlations. These models can reliably be used in designing spot-weld joints.

Acknowledgment

This paper is based on the work supported by the Scientific Research Projects of TUBITAK with Code No. 106M301 and Mercedes-Benz Turk A.S. The authors wish to thank the research staff of Mercedes-Benz Turk A.S., especially Ismail Sarioglu, for their help and support during the preparation and testing of the specimens.

References

[1] Thornton, P. H., Krause, A. R., and Davies, R. G., 1996, "The Aluminum Spot Weld," Weld. J. (Miami, FL, U.S.), **75**(3), pp. 101s–108s.
[2] Pollard, B., 1982, "Fatigue Strength of Spot Welds in Titanium-Bearing HSLA Steels," SAE International Congress and Exposition, Detroit, MI.
[3] Barkey, M. E., Kang, H., and Lee, Y. L., 2001, "Failure Modes of Single Resistance Spot Welded Joints Subjected to Combined Fatigue Loading," Int. J. Mater. Prod. Technol., **16**(6/7), pp. 510–527.
[4] Rathbun, R. W., Matlock, D. K., and Speer, J. G., 2003, "Fatigue Behavior of Spot-Welded High-Strength Sheet Steels," Weld. J. (Miami, FL, U.S.), **82**(8), pp. 207s–218s.
[5] Chao, Y. J., 2003, "Failure Mode of Spot Welds: Interfacial Versus Pullout," Sci. Technol. Weld. Joining, **8**(2), pp. 133–137.
[6] Deng, X., Chen, W., and Shi, G., 2000, "Three-Dimensional Finite Element Analysis of the Mechanical Behavior of Spot Welds," Finite Elem. Anal. Design, **35**, pp. 17–39.
[7] Wang, P. C., and Ewing, K. M., 1994, "Effect of Weld Design on the Fatigue Strength of Laser and Resistance Spot Welded Tubular T-Joints for Automotive Applications," Weld. J. (Miami, FL, U.S.), **73**(9), pp. 209s–217s.
[8] Chao, Y. J., 2003, "Ultimate Strength and Failure Mechanism of Resistance Spot Weld Subjected to Tensile, Shear, or Combined Tensile/Shear Loads," ASME J. Eng. Mater. Technol., **125**, pp. 125–132.
[9] Linder, J., and Melander, A., 1998, "Fatigue Strength of Spot Welded Stainless Sheet Steels Exposed to 3% NaCl Solution," Int. J. Fatigue, **20**(5), pp. 383–388.
[10] Henrysson, H. F., 2000, "Fatigue Life Prediction of Spot Welds Using Coarse FE Meshes," Fatigue Fract. Eng. Mater. Struct., **23**(9), pp. 737–746.
[11] Di Fant-Jaeckels, H., and Galtier, A., 2001, "Fatigue Lifetime Prediction Model for Spot Welded Structures," Rev. Metall./Cah. Inf. Tech., **1**, pp. 83–95.
[12] Xu, S., and Deng, X., 2004, "An Evaluation of Simplified Finite Element Models for Spot Welded Joints," Finite Elem. Anal. Design, **40**, pp. 1175–1194.
[13] Wonseok, J., Bae, D., and Sohn, I., 2004, "Fatigue Design of Various Type Spot Welded Lap Joints Using the Maximum Stress," KSME Int. J., **18**(1), pp. 106–113.
[14] Sheppard, S. D., and Strange, M., 1992, "Fatigue Life Estimation in Resistance Spot Welds: Initiation and Early Growth Phase," Fatigue Fract. Eng. Mater. Struct., **15**(6), pp. 531–549.
[15] Radaj, D., 1996, "Theory of Forces and Stresses in Spot Welded Overlap Joints," Arch. Appl. Mech., **67**, pp. 22–34.
[16] Pook, L. P., 1975, "Fracture Mechanics Analysis of the Fatigue Behaviour of Spot Welds," Int. J. Fract., **11**, pp. 173–176.
[17] Pan, N., and Sheppard, S., 2002, "Spot Welds Fatigue Life Prediction With Cyclic Strain Range," Int. J. Fatigue, **24**, pp. 519–528.
[18] Pan, N., 2000, "Fatigue Life Study of Spot Welds," Ph.D. thesis, Stanford University, Stanford, CA.
[19] Kan, Y. R., 1976, "Fatigue Resistance of Spotwelds—An Analytical Study," Met. Eng. Q., **16**(4), pp. 26–36.
[20] Gero, B. M., 1997, "Acousto-Ultrasonic Evaluation of Cyclic Fatigue of Spot Welded Structures," MS thesis, Virginia Polytechnic Institute and State University, Blacksburg, VA.
[21] Ertas, A. H., 2004, "Fatigue Behavior of Spot Welds," MS thesis, Bogazici University, Istanbul, Turkey.
[22] El-Sayed, M. E. M., Stawiarski, T., and Fruntiger, R., 1996, "Fatigue Analysis of Spot-Welded Joints Under Variable Amplitude Load History," Eng. Fract. Mech., **55**(3), pp. 363–369.
[23] Davidson, J. A., 1982, "A Review of the Fatigue Properties of Spot-Welded Sheet Steels," SAE International Congress and Exposition, Detroit, MI.
[24] Dannbauer, H., Gaier, C., and Hofwimmer, K., 2005, "Fatigue Analysis of Welding Seams and Spot Joints in Automotive Structures," SAE International Congress and Exposition, Detroit, MI.
[25] Adib, H., Gilbert, J., and Pluvinage, G., 2004, "Fatigue Life Duration Prediction for Welded Spots by Volumetric Method," Int. J. Fatigue, **26**, pp. 81–94.
[26] Hou, Z., Wang, Y., Li, C., and Chen, C., 2006, "An Analysis of Resistance Spot Welding," Weld. J. (Miami, FL, U.S.), **85**(3), pp. 36–40.
[27] Socie, D. F., 1977, "Fatigue-Life Prediction Using Local Stress-Strain Concepts," Exp. Mech., **17**, pp. 50–56.
[28] Zhang, S., 2001, "Approximate Stress Formulas for a Multiaxial Spot Weld Specimen," Weld. J. (Miami, FL, U.S.), **80**(8), pp. 201s–203s.
[29] Peeker, E., and Niemi, E., 1999, "Fatigue Crack Propagation Model Based on a Local Strain Approach," J. Constr. Steel Res., **49**, pp. 139–155.
[30] Roessle, M. L., and Fatemi, A., 2000, "Strain-Controlled Fatigue Properties of Steels and Some Simple Approximations," Int. J. Fatigue, **22**, pp. 495–511.
[31] Roessle, M. L., Fatemi, A., and Khosrovaneh, A. K., 1999, "Variation in Cyclic Deformation and Strain-Controlled Fatigue Properties Using Different Curve Fitting and Measurement Techniques," SAE International Congress and Exposition, Detroit, MI.
[32] Cooper, J. F., and Smith, R. A., 1985, "The Measurement of Fatigue Cracks at Spot Welds," Int. J. Fatigue, **3**, pp. 137–140.
[33] Davidson, J. A., and Imhof, E. J., 1983, "A Fracture Mechanics and System-Stiffness Approach to Fatigue Performance of Spot-Welded Sheet Steels," SAE International Congress and Exposition, Detroit, MI.
[34] Newman, J. A., and Dowling, N. E., 1998, "A Crack Growth Approach to Life Prediction of Spot-Welded Lap Joints," Fatigue Fract. Eng. Mater. Struct., **21**, pp. 1123–1132.
[35] Stephens, R. I., Fatemi, A., Stephens, R. R., and Fuchs, H. O., 2001, *Metal Fatigue in Engineering*, Wiley-Interscience, New York.
[36] Suresh, S., 2004, *Fatigue of Materials*, Cambridge University Press, Cambridge.
[37] Cui, W., 2002, "A State of the Art Review on Fatigue Life Prediction Methods for Metal Structures," J. Mar. Sci. Technol., **7**, pp. 43–56.
[38] Schijve, J., 2001, *Fatigue of Structures and Materials*, Wiley-Interscience, New York.
[39] Zhou, M., Hu, S. J., and Zhang, H., 1999, "Critical Specimen Sizes for Tensile-Shear Testing of Steel Sheets," Weld. J. (Miami, FL, U.S.), **78**(9), pp. 305s–313s.
[40] Ong, J. H., 1993, "An Improved Technique for the Prediction of Axial Fatigue Life From Tensile Data," Int. J. Fatigue, **15**(3), pp. 213–219.
[41] Gean, A., Westgate, A., Kucza, J. C., and Ehrstrom, J. C., 1999, "Static and Fatigue Behavior of Spot-Welded 5182-O Aluminum Alloy Sheet," Weld. J. (Miami, FL, U.S.), **78**(3), pp. 90s–96s.
[42] Achintya, H., and Sankaran, M., 2000, *Probability, Reliability and Statistical Methods in Engineering Design*, Wiley, New York.
[43] Tryon, R. G., and Cruse, T. A., 1998, "A Reliability-Based Model to Predict Scatter in Fatigue Crack Nucleation Life," Fatigue Fract. Eng. Mater. Struct., **21**, pp. 257–267.
[44] Wirsching, P. H., 2006, "Application of Reliability Methods to Fatigue Analysis and Design," *Recent Developments in Reliability-Based Civil Engineering*, World Scientific, New York, pp. 125–140.
[45] ANSYS User's Manual, Version 9.0, ANSYS Software Inc., 2004.
[46] Salvini, P., Vivio, F., and Vullo, V., 2000, "A Spot Weld Finite Element for Structural Modeling," Int. J. Fatigue, **22**(8), pp. 645–656.
[47] Chang, B., Shi, Y., and Dong, S., 1999, "Comparative Studies on Stresses in Weld-Bonded, Spot-Welded, and Adhesive-Bonded Joints," J. Mater. Process. Technol., **87**, pp. 230–236.

Downloaded 26 Dec 2008 to 193.140.210.85. Redistribution subject to ASME license or copyright; see http://www.asme.org/terms/Terms_Use.cfm